SI Appendix

SI Figures

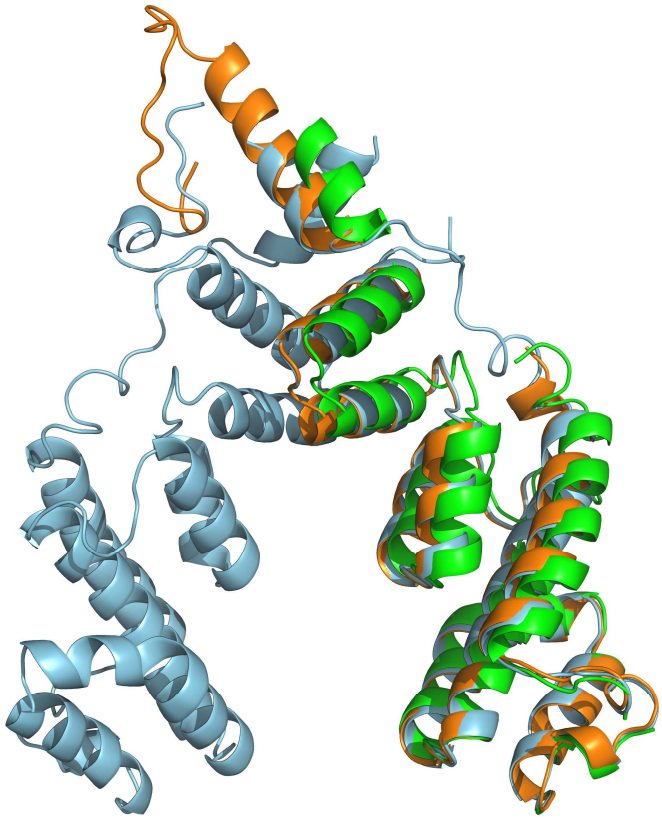

Figure S1: TPL has a CRA domain. Superimposition of two proteins possessing the LisH-CTLH-CRA domains (the human RAN-Binding protein 9 [Uniprot Q96S59, green], and a protein from the unicellular algae *C. reinhardtii* [Uniprot A8HQD2, orange] on AtTPL184 structure (blue): Models were generated using PHYRE^2 (1).

Based on sequence similarity, the CRA domain is detected in numerous proteins containing the LisH and CTLH domains (see Table S5). However, there was no structure available for a CRA domain. When using PHYRE^2(1), we realized that the CRA domain of all LisH-CTLH-CRA containing proteins was modelled with a high confidence to the C-terminal region of TPL184/TPR2 structures (see Table S5). This analysis revealed that the TPL/TPR2 structures provided the first structure for a CRA domain and that TPL/TPR2 both possessed a CRA domain that had remained unnoticed.

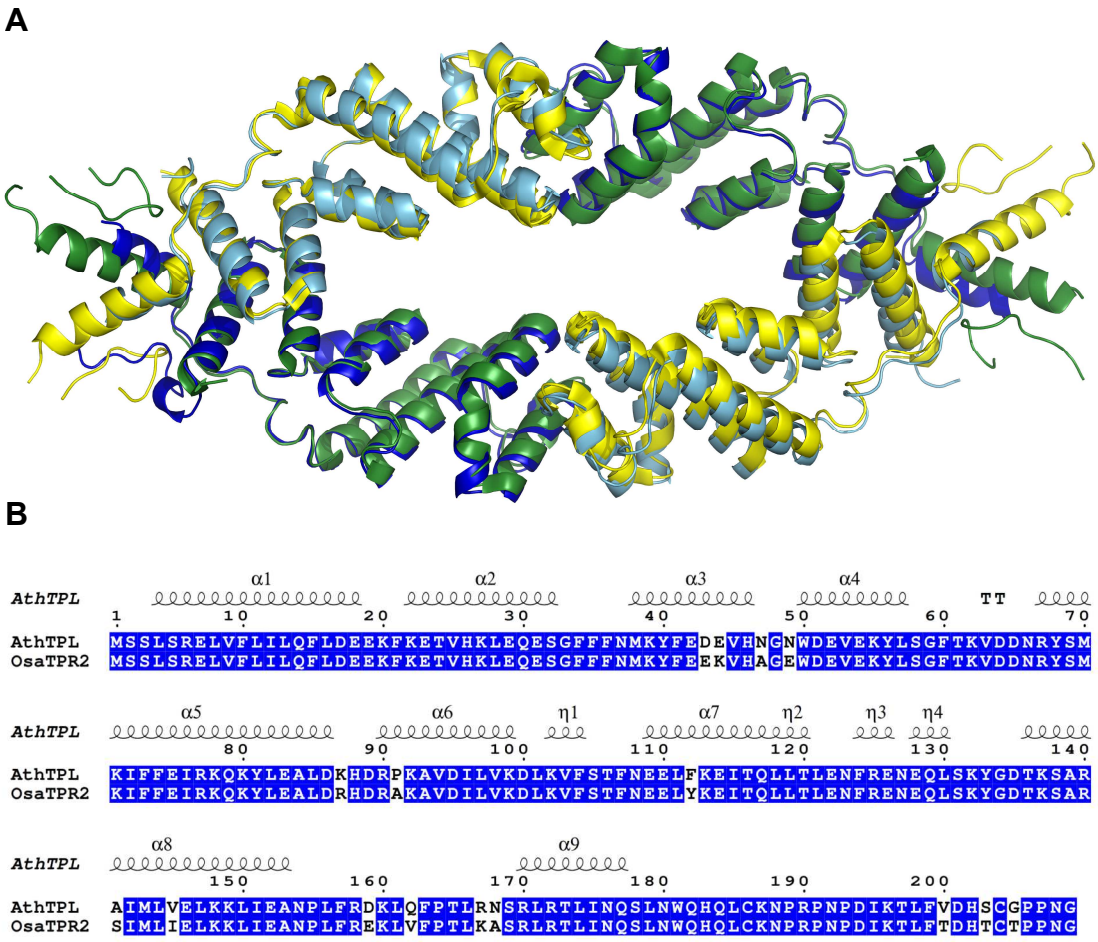

Figure S2: Structural comparison of AtTPL with OsTPR2. (A) Superimposition of the tetramers of AtTPL (light and dark blue) and OsTPR2 (yellow and dark green) (5C7F) showing the high similarity between both structures. The AtTPL184 structure has an rmsd of 0.7 Å for 179 Cα using DALI with the OsTPR2 structure. (B) Sequence alignment of the N-terminal part of AtTPL and OsTPR2 using ESPript with Multalin (2) and ESPript 3.0 (3). These sequences show 92% identity.

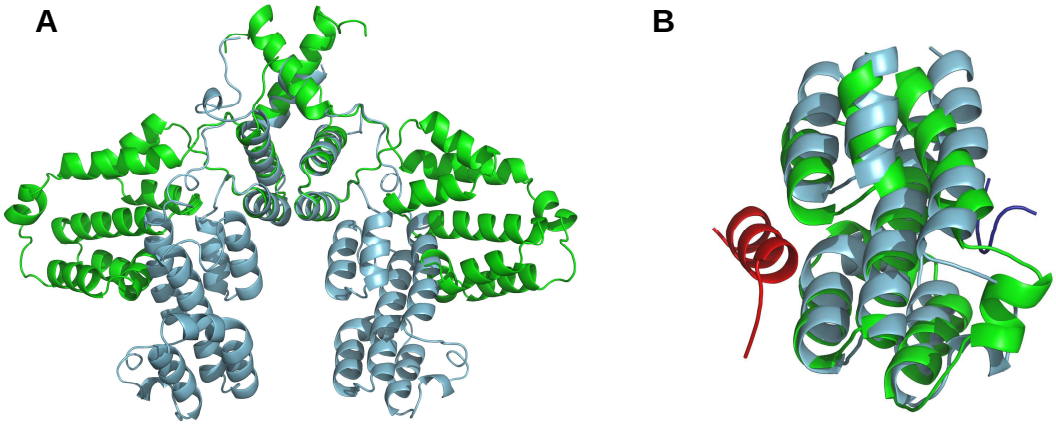

Figure S3: Structural comparison of AtTPL with Smu1. (A) Superimposition of the dimer of Smu1 (5EN8) (green) and AtTPL184 (blue) with overlay of the LisH domains. (B) Superimposition of the CRA/CTLH domain of Smu1 interacting with the RED peptide (red) and the CRA/CTLH domain of AtTPL184 interacting with IAA27 (dark blue). The LisH and the CTLH/CRA domains of TPL show a high similarity with Smu1 domains but their relative positions are different between Smu1 and TPL (4).

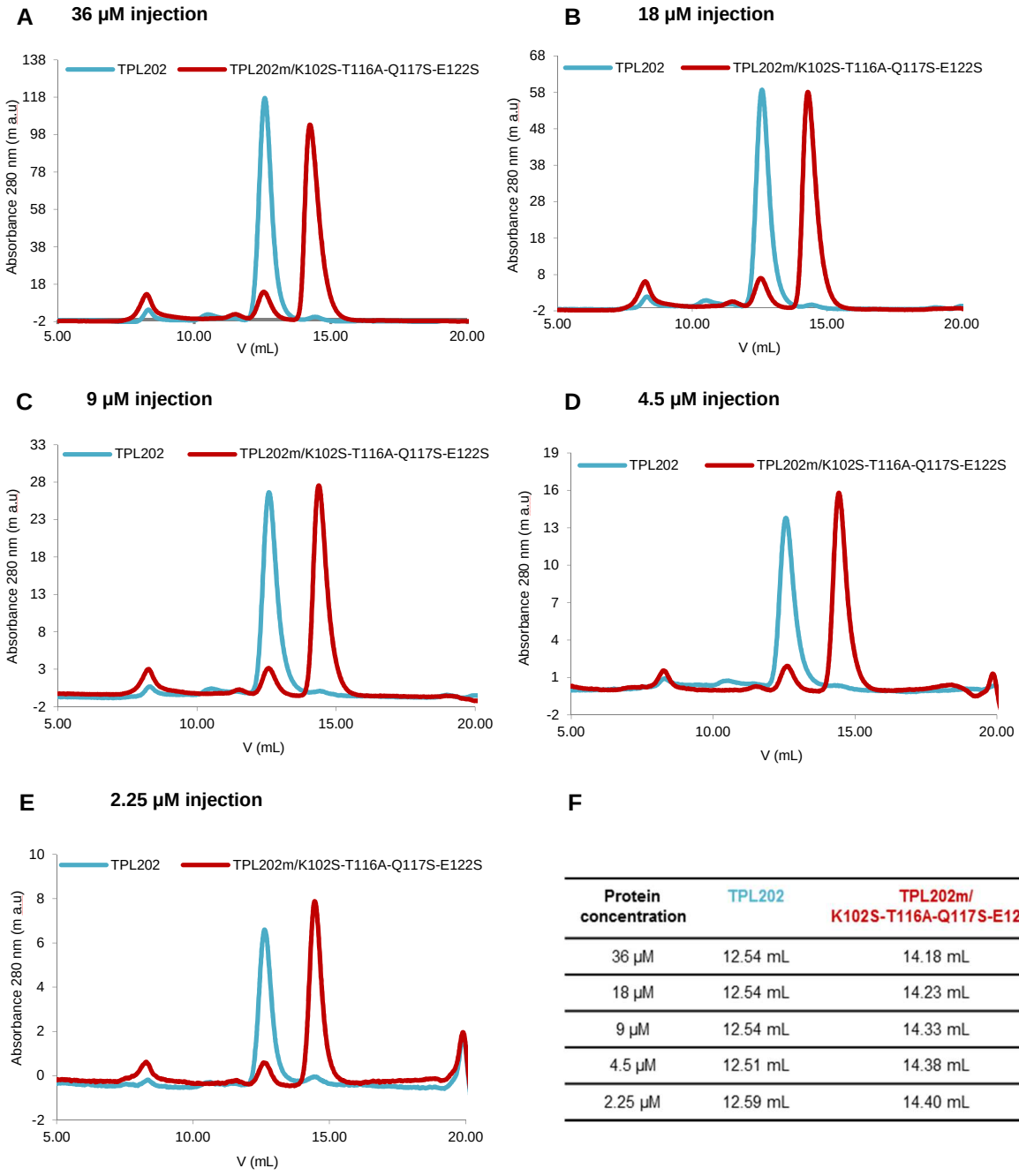

F

Protein concentration	TPL202	TPL202m/ K102S-T116A-Q117S-E122S
36 µM	12.54 mL	14.18 mL
18 µM	12.54 mL	14.23 mL
9 µM	12.54 mL	14.33 mL
4.5 µM	12.51 mL	14.38 mL
2.25 µM	12.59 mL	14.40 mL

Figure S4: Analysis of TPL oligomerization state by SEC. (A-E) Elution profiles of TPL202 (blue) and the dimeric mutant TPL202m/K102S-T116A-Q117S-E122S (red) in a Superdex-S200 increase (GE Healthcare) size-exclusion chromatography column. (F) Elution volumes (mL) of both proteins at different concentrations showing that TPL202 elutes at a tetramer independently of the protein concentration. These experiments have been made at low protein concentrations (2.25 µM - 36 µM) in comparison with the SEC-MALLS experiments [36 µM (1 mg/mL) – 432 µM (12 mg/mL)].

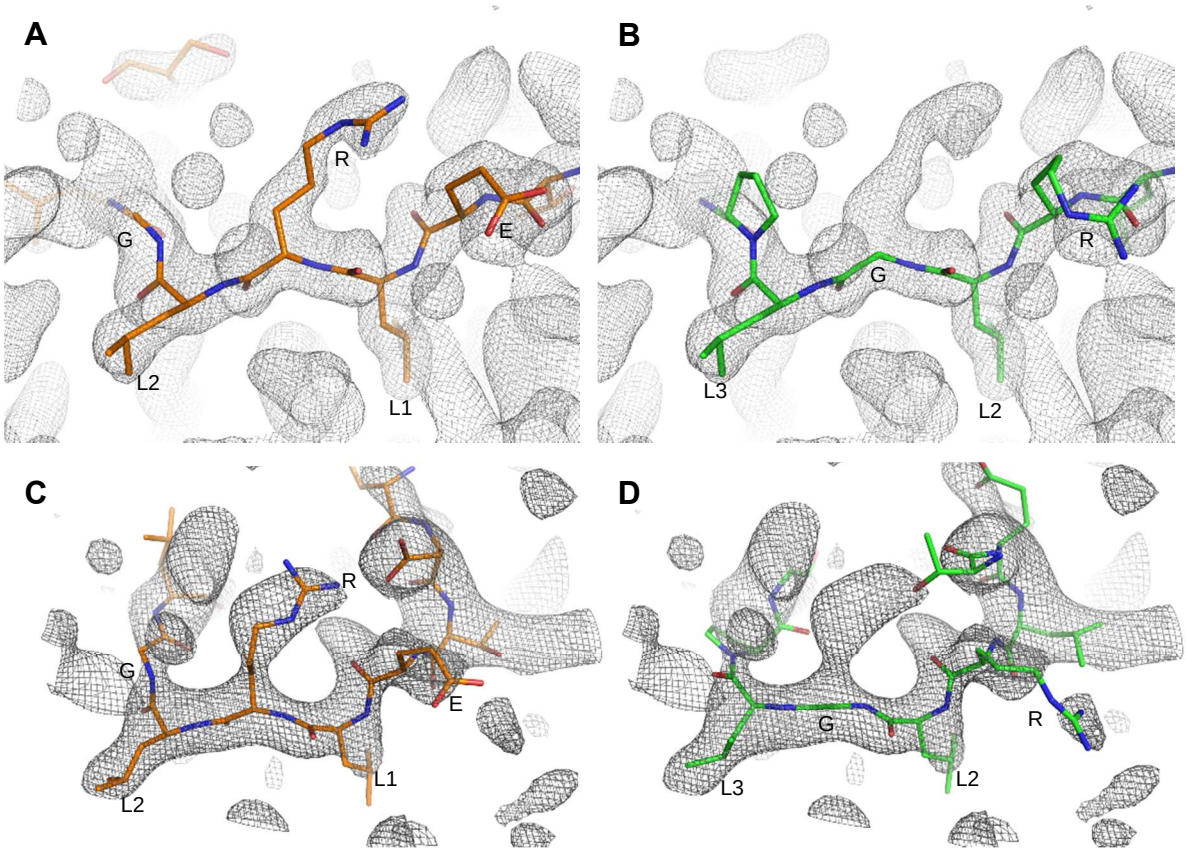

Figure S5: Comparing IAA peptide registers between OsTPR2 and AtTPL data. 2Fo-Fc simulated annealed omit electron density map is shown as a grey mesh contoured at one standard deviation above the mean electron density value. In (A) and (B) the electron density for AtTPL184 is shown. The peptide register that we propose is shown in orange sticks in (A). Note the excellent fit in particular of the Arginine residue. In (B), the green sticks represent the peptide register as proposed by Ke *et al.* (5). In (C) and (D), the electron density of the data deposited by Ke *et al.* is shown. The orange model in (C) represents the Ke *et al.* (5) peptide re-modelled using our proposed peptide register whereas the green model in (D) is the peptide as modelled by Ke *et al.*(5).

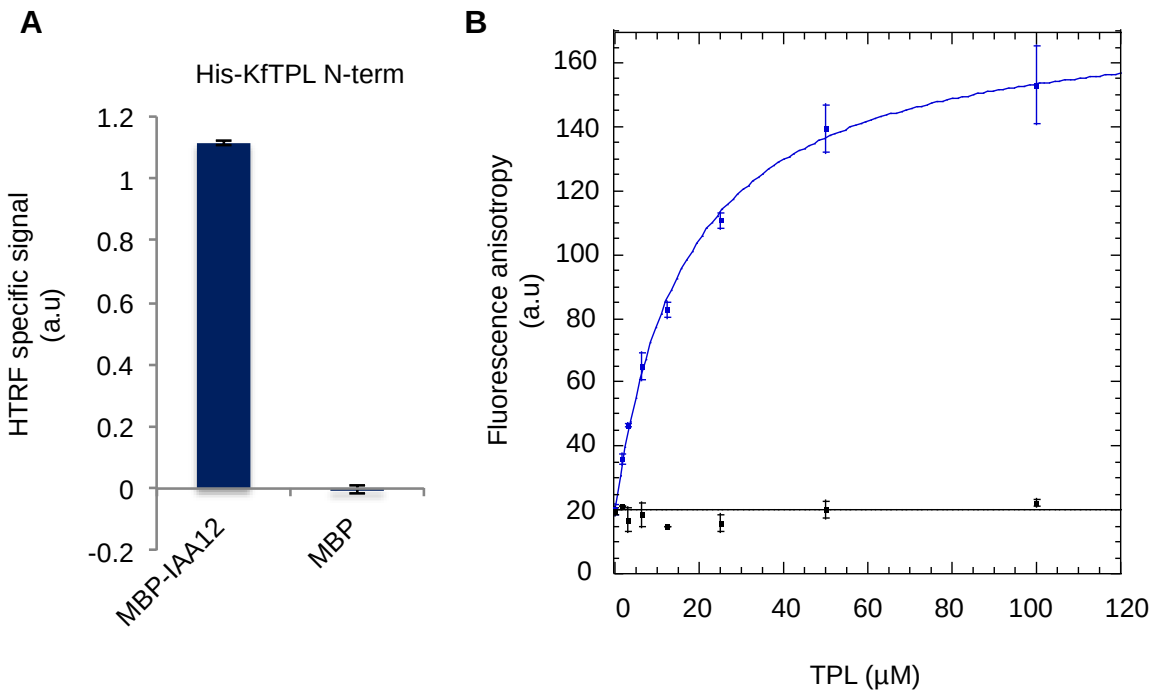

Figure S6: Evolutionary conservation of TPL interactions. (A) HTRF interaction assay showing the interaction between the N-terminus of *Klebsormidium flaccidum* TPL and AtIAA12 repressor (n = 3; error bars = SD) (B) Anisotropy interaction assay between KfTPL N-terminus and the FAM-IAA12 EAR peptide (blue) or its mutant version mIAA12 (black) (Table S4). EC_{50} for IAA12-EAR = 16.78 µM ± 1.24 (n = 3; error bars = SD).

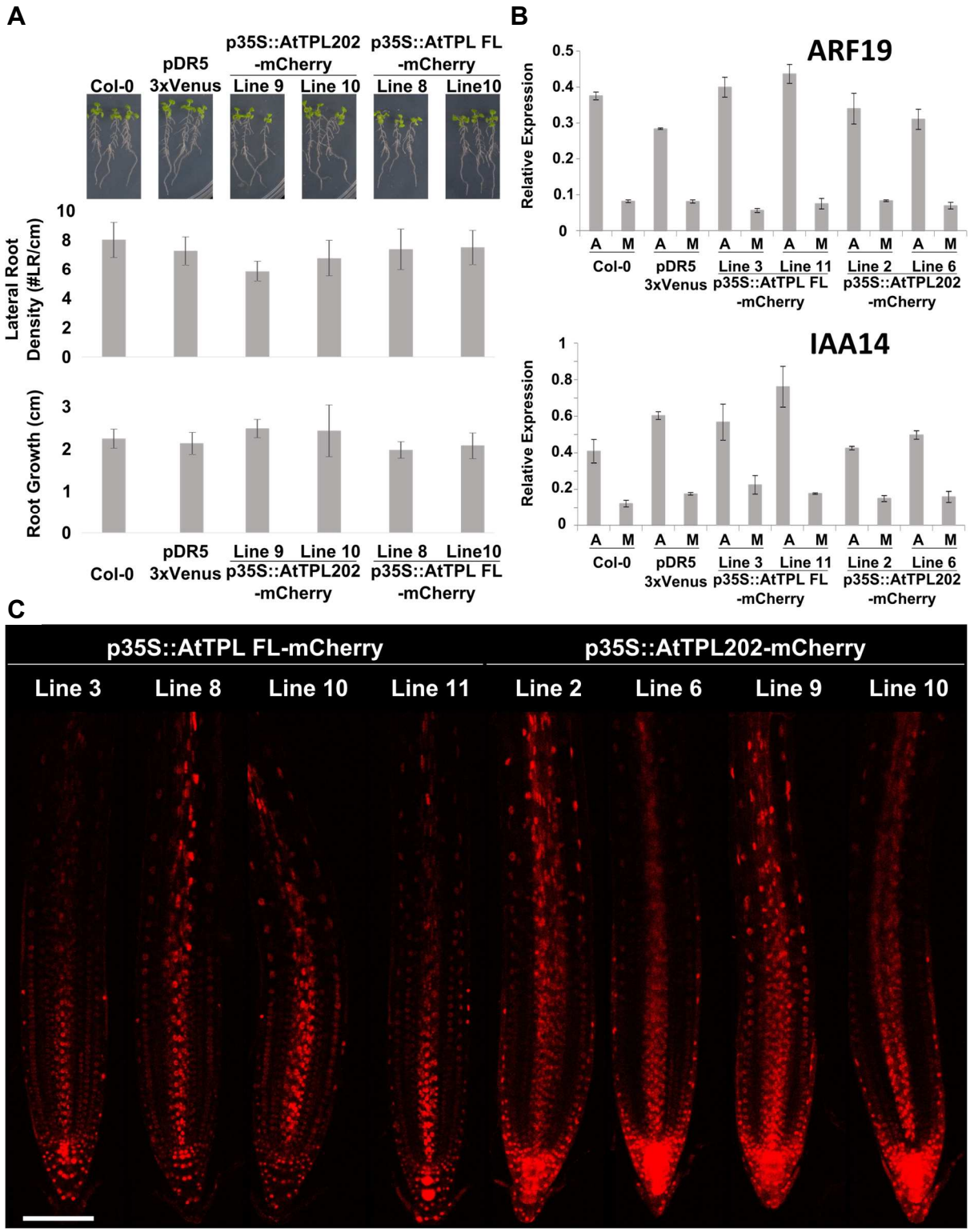

Figure S7: TOPLESS overexpression lines are not affected in their auxin responsiveness. (A) Auxin-dependent effects on root growth and lateral root formation was analyzed in 2 independent transgenic arabidopsis lines overexpressing full-length TPL or TPL202. Root growth and lateral root density were determined 5 days after transfer on auxin (NAA 100 nM, n = 10 seedlings). (B) Auxin responses at

the transcriptional level was analyzed in 2 independent overexpression lines of full length TPL or TPL202. *ARF19* and *IAA14* mRNA relative expression were determined 2 hours after transfer on auxin (M: Mock, A: Auxin (NAA 1µM), n = 2 biological replicates). (C) Confocal laser scanning images of root tips of the lines used in the experiments showing relatively identical TPL-mCherry fluorescence levels (scale bar = 100 µm). Basta-resistant T2 seedlings were used in all experiments and basta-resistant pDR5::3xVenus were used as controls. Col-0 seedlings grown in the absence of basta were also used as controls.

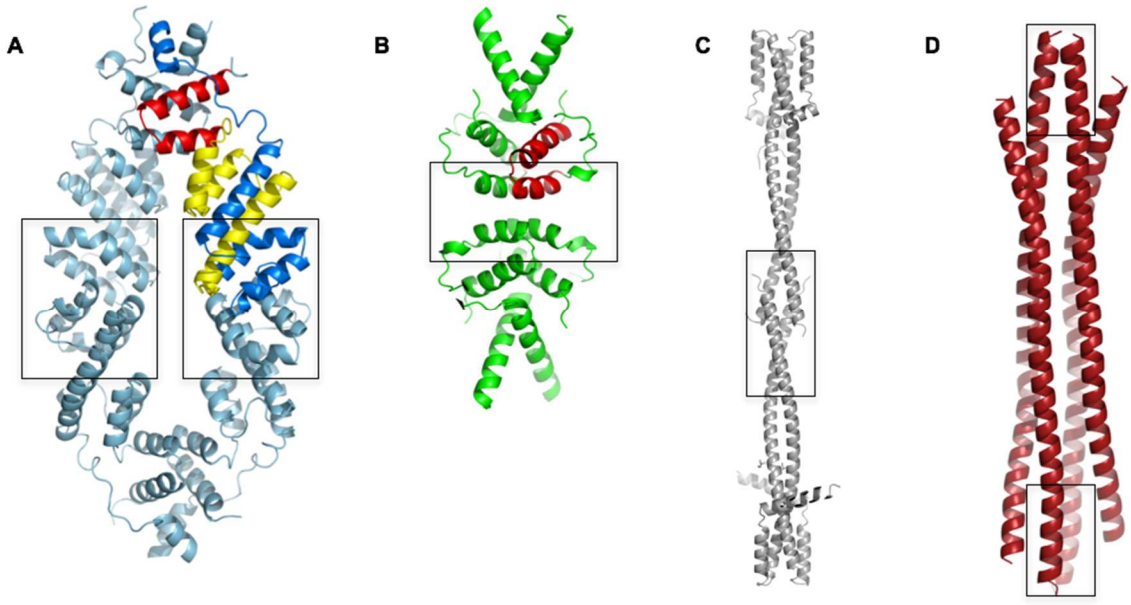

Figure S8: Different tetramerization modes of co-repressors. (A) AtTPL184 tetramer with LisH in red, CTLH in yellow and CRA in marine blue on one of the monomers. (B) Human TBL1 (2XTC) tetramer with LisH in red on one of the monomers (6). (C) Human TLE (4OM3) (7). (D) Yeast TUP1p (3VP8) tetramer (8). Tetramerization interfaces framed with a black rectangle.

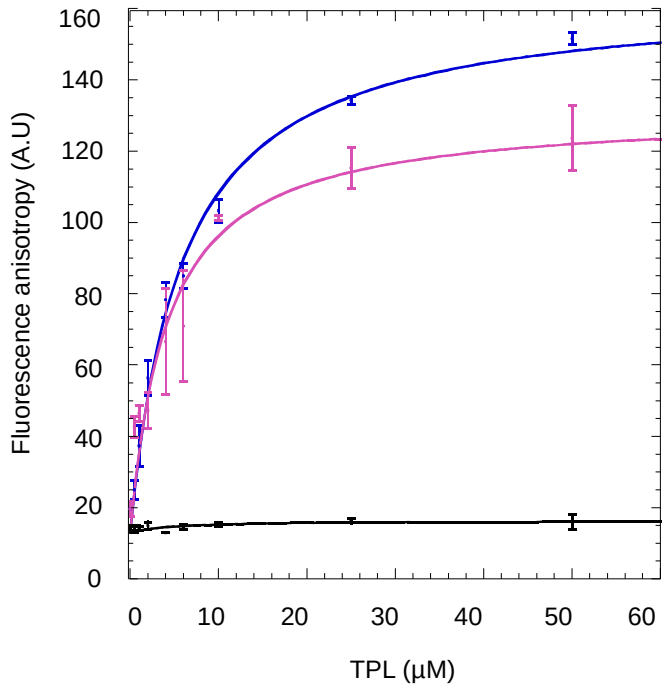

Figure S9: G2 mutant maintains its capacity to interact with EAR motifs. Fluorescence anisotropy experiment done with FAM-IAA12 EAR peptide or its mutant version mIAA12 (black) (Table S4) showing that TPL202 (blue) and TPL202m/F35Q G2 (pink) similarly interact with LxLxL-type EAR motifs. TPL202 EC50 = 5.8 µM ± 0.6; TPL202m/F35Q G2 = 4.2 µM ± 1.1 (n = 3; error bars = SD).

SI Tables

	Peak Se*	Apo	IAA peptide
Wavelength, Å	0.9723	0.8732	0.9762
Beamline	ESRF ID29	ESRF ID23-EH2	ESRF ID29
Resolution range, Å	56.76-2.92 (3.03 - 2.92)	23.93-2.61 (2.70 - 2.61)	28.51-1.95 (2.02 - 1.95)
Space group	P 4_3 2_1 2	P 3_1 1 2	P 4_3 2_1 2
Unit cell axes a,b,c in Å	99.1 99.1 290.0	72.7 72.7 181.1	94.1 94.1 298.0
Total reflections	416016 (32760)	115884 (10928)	709574 (70881)
Unique reflections	32181 (3051)	16927 (1677)	96694 (9366)
Multiplicity	12.9 (10.7)	6.8 (6.5)	7.3 (7.6)
Completeness, %	97 (97)	100 (100)	98 (97)
Mean I/sigma(I)	10.14 (1.45)	12.21 (1.79)	13.11 (1.01)
Wilson B-factor, Å²	58.58	57.68	36.99
R-merge	0.2253 (1.718)	0.1059 (0.8868)	0.09131 (2.316)
R-meas	0.2346 (1.802)	0.1144 (0.9624)	0.09837 (2.485)
CC1/2	0.996 (0.571)	0.998 (0.657)	0.999 (0.47)
CC*	0.999 (0.853)	1 (0.89)	1 (0.8)
Reflections used in refinement		16924 (1679)	96685 (9365)
Reflections used for R-free		857 (91)	4830 (441)
R-work, %		20.3 (28.4)	18.5 (36.9)
R-free, %		25.8 (34.7)	21.3 (39.1)
CC(work)		0.955 (0.791)	0.965 (0.740)
CC(free)		0.934 (0.572)	0.939 (0.655)
Number of non-hydrogen atoms		3060	6965
Macromolecules		3029	6359
Ligands			76
Protein residues		357	755
RMS(bonds), Å		0.014	0.014
RMS(angles), °		1.71	1.50
Ramachandran favored (%)		98	98
Ramachandran allowed (%)		1.7	2
Ramachandran outliers (%)		0	0.13
Rotamer outliers (%)		6.5	2
Clashscore		2.14	0.70
Average B-factor		62.22	50.75
Macromolecules		62.29	50.14
Ligands			67.12
Solvent		55.90	55.61

Table S1: Data collection and refinement statistics. Outer shell range and statistics are indicated in parentheses.

A	Concentration ($mg.mL^{-1}$)	MW (kDa)	Number of monomers-Quaternary state
AtTPL184	2	95	3.7-tetramer
AtTPL202	1	102.4	3.7-tetramer
	2	103	3.7-tetramer
	4	103	3.7-tetramer
B	**Tetramerization interface I mutants**		
TPL202m/K102S-T116A-Q117S-E122S	2	50.4	1.8-dimer
TPL202m/Q117M-E122T	2	102	3.7-tetramer
TPL202m/Q117S-E122S	2	99.6	3.6-tetramer
TPL202m/T116A	2	72	2.6-equilibrium
	4	78.8	2.9-equilibrium
	6	81.2	3.0-equilibrium
	12	85.3	3.1-equilibrium
TPL202m/K102S	1	87.6	3.2-equilibrium
	2	91.2	3.3-equilibrium
	6	96.9	3.5-equilibrium
C	**Tetramerization interface II mutants**		
TPL202m/N176H	2	103	3.7-tetramer
TPL202m/R172S	2	99	3.6-tetramer
D	**Groove 3 mutants**		
TPL202m/Y68A	2	106	3.8-tetramer
TPL202m/F74Q	2	55	2.0-dimer
TPL202m/L130A	2	55.4	2.0-dimer
TPL202m/Y133A	2	55.4	2.0-dimer
E	**AtTPL202 + EAR motifs**		
+IAA12 EAR motif	2	109.3	3.9-tetramer
+IAA27 EAR motif	2	107.3	3.9-tetramer

Table S2: Quaternary structure of AtTPL184 and AtTPL202 (wild type and mutant forms) determined by SEC-MALLS.

	K102/ T120	T120/ K102	Q117/ T116	Q117/ Q117	K113/ Q117	Q117/ K113	E122/ K102
TPL A/B	+	+	+				
TPL C/D	+	+		+	+	+	
5C7F A/C	+	+		+			
5C7F B/D	+	+		+			
4ZHE A/B	+	+					+
4ZHE D/C	+	+		+			
5C6V A/C	+	+		+			
5C6V B/D	+	+		+			
5C7F A/C	+	+		+			
5C7F B/D	+	+		+			

Table S3: Interaction (lower than 3.5 Å) observed in tetramer interfaces for AtTPL and OsTPR2 (3). TPL: AtTPL/IAA27; 5C7F: OsTPR2/IAA1; 4ZHE: OsTPR2/SeMet; 5C6V: OsTPR2/NINJA; 5C7F: Os-TPR2/IAA10.

EAR peptide	Sequence	
FAM-IAA12	ESELELGLGLSL	Used for anisotropy
FAM-mIAA12	ESEAEAGAGASA	Used for anisotropy
IAA12 long	KSNLPAESELELGLGLSL	Used for SEC-MALLS
IAA27	TELRLGLPGSE	Used for crystallography and SEC-MALLS

Table S4: EAR peptides sequences used in this study.

Uniprot	ATG number/name	length	Domain	Function	Model (confidence)	G3/G4
Q94AI7	AT1G15750/TPL	1131	LisH/CTLH/WD40/WD40	Repression	TPR2(100)/Smu1(100)	Y/N
Q0WV90	AT1G80490/TPR1	1120	LisH/CTLH/WD40/WD40	Repression	TPR2 (100)/Smu1(100)	Y/N
Q9LRZ0	AT3G16830/TPR2	1131	LisH/CTLH/WD40/WD40	Repression	TPR2(100)/Smu1(100)	Y/N
Q84JM4	AT5G27030/TPR3	1108	LisH/CTLH/WD40/WD40	Repression	TPR2(100)/Smu1(100)	Y/N
Q27GK7	AT3G15880 /TPR4	1135	LisH/CTLH/WD40/WD40	Repression	TPR2(100)/Smu1(100)	Y/N
Q9FNN2	At5g08560	589	LisH/CTLH/WD40		TPR2(100)/Smu1(100)	Y/N
Q9FND4	AT5G43920	524	LisH/CTLH/WD40		TPR2(100)/Smu1(100)	Y/N
Q8W117	AT1G73720/smu1	511	LisH/CTLH/WD40	Splicing	TPR2(99.4)/Smu1(99.8)	N/Y
Q0WVR3	At2g25420/TPR-like	740	LisH/CTLH/LisH/CTLH/WD40		TPR2(99.9)/Smu1(99.8)	Y/N
Q9LXC7	At5g09630	386	LisH/CTLH/CRA/RING		TPR2(99.6)/Smu1(99.7)	Y/N
Q9ZQ45	At2g22690	381	LisH/CTLH/CRA/RING		TPR2(99.6)/Smu1(99.4)	N/N
Q9T075	At4g37880	388	LisH/CTLH/CRA/RING		TPR2(99.6)/Smu1(99.4)	N/N
Q9M2V9	At3g55070	418	LisH/CTLH/CRA/RING		TPR2(99.6)/Smu1(99.3)	N/N
F4HYD7	At1g35470/RanBPM	467	SPRY/LisH/CTLH/CRA		TPR2(99.8)/Smu1(99.8)	Y/N
Q8RX25	At4g09200	397	SPRY/LisH/CTLH/CRA		TPR2(99.8)/Smu1(100)	Y/N
Q8LF14	AT4G09340	429	SPRY/LisH/CTLH/CRA		TPR2(100)/Smu1(99.8)	Y/N
Q8GX44	At1g11110	227	LisH/CTLH/CRA		TPR2(99.9)/Smu1(99.9)	N/N
Q8GYP0	At4g09300	224	LisH/CTLH/CRA		TPR2(99.9)/Smu1(99.9)	Y/Y
A8MQF1	AT1G61150	226	LisH/CTLH/CRA		TPR2(100)/Smu1(100)	Y/N
Q9LNE1	At1g06060	213	LisH/CTLH/CRA		TPR2(99.9)/Smu1(99.9)	N/N
F4K250	At5g66810	750	CTLH/CRA/CTLH/CRA		TPR2(98.9)/Smu1(98.0)	Y/N
Q9SMS2	AT4g09330	111	CRA			
O48847	AT2G32700/LUH	787	LisH/WD40	Repression	LisH: TBL1	
Q9FUY2	AT4G32551/LEUNIG	931	LisH/WD40	Repression	LisH: TBL1	
Q9M086	At4g31160/DCAF1	1883	LisH/WD40	Ubiquitination	LisH: TBL1	
Q9FN19	AT5g67320/HOS15	613	LisH/WD40	histone deacetyl.	LisH: TBL1	
Q9LU74	AT5g57120/MUL3	330	LisH/SRP40		LisH: Lis-1	
Q8VYW7	AT5g16210/T21H19	1180	LisH/LisH/Armadillo/Armadillo		LisH: TBL1	
Q9FQ24	AT3G55005/TON 1b	257	LisH	microtubule org.	LisH: TBL1	
Q9FQ25	AT3G55000/TON 1a	260	LisH	microtubule org.	LisH: TBL1	
Examples of proteins from other eukaryotes						
Chlamydomonas reinhardtii						
A8HQD2	CRDRAFT-136822	232	LisH/CTLH/CRA		TPR2(100)/Smu1(100)	Y/N
Homo sapiens						
Q96S59	Hs708182	729	SPRY/LisH/CTLH/CRA	Adapter protein	TPR2(99.6)/Smu1(99.6)	Y/N

Table S5: Model of LisH domain containing proteins in *A. thaliana.* Uniprot number, ATG number, length (aa) and predicted domains are indicated. Modeling was performed with PHYRE2 (1). All LisH-CTLH (with an extra WD40) and LisH-CTLH-CRA can be modeled with the N-ter of OsTPR2 or *Caenorhabditis elegans* Smu1 as template with a confidence between 98.0% and 100% (indicated with brackets). These proteins are highly similar to the N-terminus of TPL/TPR2 or Smu1. Most of them contain a hydrophobic groove 3 (G3: Y) found in TPL/TPR2 whereas few contain a hydrophobic groove 4 (G4: Y) specific of Smu1, both potentially involved in protein binding. Some of the modeled proteins contain also a potential tetramer interface (not

shown). Proteins predicted to contain only a LisH domain were modeled with the LisH domain of TBL1 or Lis-1 as template. Two examples of proteins from *C. reinhardtii* and *H. sapiens* shown in Fig. S1 are also indicated.

Name	Strand	Sequence	Experiment
TPL(FL)	Forward Reverse	5' CACCATGTCTTCTCTTAGTAGAGAGCTC 3' 5' TCTCTGAGGCTGATCAGATGC 3'	Repression assay
TPL202 (and mutant)	Forward Reverse	5' CACCATGAAACATCACCATCACCATC 3' 5' TTAAGAGTGATCCACAAAAAGAGTC 3'	Repression assay
IAA12-DI	Forward Reverse	5' CACCATGCGTGGTGTGTCAGAATTG 3' 5' TCAACTGTTCATCCTGTGTAACCCA 3'	Y2H
WUS	Forward Reverse	5' CACCATGGAGCCGCCACAGCATC 3' 5' CTAGTTCAGACGTAGCTCAAGAGAAG 3'	Y2H
AtTPL202	Forward Reverse	5' GGCGCCATGGGCTCTTCTCTTAGTAGAGAGCTC 3' 5' CGTGCGGCCGCTTAAGAGTGATCCACAAAAAGAGTC 3'	HTRF,Anisotropy, SEC-MALLS
AtTPL202 m/ L130A	Forward Reverse	5' AACTTCCGGGAGAATGAACAGGCCTCCAAGTATGGGGACACCAAG 3' 5' CTTGGTGTCCCCATACTTGGAGGCCTGTTCATTCTCCCGGAAGTT 3'	HTRF,Anisotropy, SEC-MALLS
AtTPL202 m/ Y133A		5' TGCAGACTTGGTGTCCCCAGCCTTGGACAGCTGTTCATTCTCCCGGAAG 3' 5' CTTCCGGGAGAATGAACAGCTGTCCAAGGCTGGGGACACCAAGTCTGCA 3'	HTRF,Anisotropy, SEC-MALLS
AtTPL202 m/ T166A	Forward Reverse	5' GTTCTCCAATGTCAACAGCTGTGCTATTTCCTTGAAAAGCTCCTCATT 3' 5' AATGAGGAGCTTTTCAAGGAAATAGCACAGCTGTTGACATTGGAGAAC 3'	HTRF,Anisotropy, SEC-MALLS
AtTPL202 m/K102S	Forward Reverse	5'GCTCCTCATTAAAAGTTGAAAACACTGACAGATCTTTCACTAGTATATCCACA GCCTTGGGAC 3' 5'GTCCCAAGGCTGTGGATATACTAGTGAAAGATCTGTCAGTGTTTTCAACTTTT AATGAGGAGC 3'	HTRF,Anisotropy, SEC-MALLS
AtTPL202 m/Q117S-E122S	Forward Reverse	5'GTTCATTCTCCCGGAAGTTCGACAATGTCAACAGCGATGTTATTTCCTTGAA AAGCTCCTCATTAAAA 3' 5'TTTTAATGAGGAGCTTTTCAAGGAAATAACATCGCTGTTGACATTGTCGAACT TCCGGGAGAATGAAC 3'	SEC-MALLS
AtTPL202 m/R172S	Forward Reverse	5'-CTCTTAGAAATTCAAGGCTGTCGACTTTGATCAACCAGAGCT-3' 5'-AGCTCTGGTTGATCAAAGTCGACAGCCTTGAATTTCTAAGAG-3'	SEC-MALLS
qCTL1	Forward Reverse	5'- AGTGGAGAGGCTGCAGAAGA-3' 5'- CTCGGGTAGCACGAGCTTTA-3'	qPCR
qARF19	Forward Reverse	5'- CACCGATCACGAAAACGATA-3' 5'- TGTTCTGCACGCAGTTCAC-3'	qPCR
qIAA14	Forward Reverse	5'- CAAAGATGGTGACTGGATGC-3' 5'- GCATGACTCGACAAACATCG-3'	qPCR

Table S6: DNA probes used for plasmid constructions.

SI Materials and Methods

Vectors construction

AtTPL184 cDNA was directly cloned from an AtTPL full-length synthetic coding sequence (Thermo Fisher). AtTPL202 cDNA was obtained by PCR from AtTPL full-length clone using oligonucleotides listed in Table S6. Both constructs were cloned into pETM11 plasmid (EMBL) for the production of N-terminal His-tagged proteins. Mutants were constructed either by site-directed mutagenesis using oligonucleotides referenced in Table S6 or by a restriction-site strategy with synthetic DNA (GeneCust) including the desired mutation.

N-terminal MBP-tagged AtTPL202 wild-type (wt) and mutated constructs were obtained by cloning the corresponding sequences into pETM40 plasmid (EMBL).
IAA12 cDNA was cloned into plasmid pETM33 (EMBL) for the production of full-length N-terminal GST-tagged proteins.
For Yeast-2-Hybrid (Y2H) and repression assays, wt and mutated AtTPL202, IAA12-DI and WUSCHEL coding sequences were amplified with specific primers (Table S6) and cloned into pENTRD-TOPO® using CACC strategy. To test in Y2H assay the interactions between AtTPL202 and repressors, AtTPL202 and its mutated versions cDNAs were cloned into bait vector pGBKT7 (Clontech), whereas IAA12-DI and WUSCHEL coding sequences were cloned into prey vector pACT2 (Clontech).
For repression assays, p35S::AtTPL-mCherry expression constructs were obtained by triple LR reactions performed with Gateway® recombination technology on the *35S* promoter, AtTPL FL, or AtTPL202 wt and mutants cDNAs, and the transfection marker mCherry in the destination vector pDESTR4-R3.
For in planta assays, p35S::AtTPL-mCherry expression constructs were obtained by triple LR reactions performed with Gateway® recombination technology on the 35S promoter, AtTPL FL, or AtTPL202 wt and the fluorescent marker mCherry in the destination vector pB7m34 with basta resistance as a selectable marker. Arabidopsis Col-0 plants were transformed with the constructs and basta-resistant T2s were used in all experiments.

Protein expression and purification

All proteins were expressed in *Escherichia coli* Rosetta 2 strain. Bacteria cultures were grown at 37ºC until they achieved an OD_{600nm} of 0.6-0.9. Protein expression was induced with isopropyl-β-D-1-thyogalactopiranoside (IPTG) at a final concentration of 400 µM at 18 °C overnight. Bacteria cultures were centrifuged and the pellets were resuspended in the buffers as indicated below, where cells were lysed by sonication.
His-tagged AtTPL184 and AtTPL202 (wt and mutants) bacteria pellets were resuspended in buffer A (CAPS 200 mM pH 10.5, NaCl 500 mM, TCEP 1 mM) with EDTA-free antiprotease (Roche). The soluble fractions recovered after sonication were passed through a Ni-sepharose (GE Healthcare) column previously washed with buffer A and the bound proteins were eluted with buffer A with 300 mM imidazole. A second purification step was carried out on Gel filtration Superdex 200 16/60 (GE Healthcare) equilibrated with buffer A.

Production of selenomethionine (Se-Met) TPL184 for crystallography was done in *E. coli* B834 (DE3) (met-) strain (Novagen) transformed with the AtTPL184 plasmid. Bacteria cultures were grown at 37 °C under agitation up to an OD_{600nm} of 0.3. Next, bacteria cultures were recovered by centrifugation and the pellets were washed twice with 100 mL of M9 minimal medium (NaH_4Cl 37 mM, KH_2PO_4 44 mM and Na_2HPO_4-$7H_2O$ 180 mM). Bacteria cultures were re-started after this at 37 °C until an OD_{600nm} of 0.6 in 1 L of 2X M9 minimal medium supplemented with MgSO4 (2 mM), FeSO4 (25 mg/L), glucose (4 g/L), vitamins (thiamine, pyridoxine, riboflavin and niacinamide at 1 mg/L), and mix of all amino acids (895 mg/L) except methionine. The expression of the Se-Met protein was induced by addition of 400 µM IPTG and Se-Met (40 mg/L). The protein was further purified in buffer B (CAPS 200 mM pH 10.5, NaCl 1 M, TCEP 1 mM) with EDTA-free antiprotease (Roche) as described above for AtTPL184.

MBP-tagged IAA12 bacteria pellets were resuspended in buffer C (Tris-HCl 20 mM pH 8, TCEP 1 mM) with EDTA-free antiprotease (Roche). Protein purification was done from the soluble fraction in an amylose-resin (GE Healthcare) column previously equilibrated with buffer C and from which bound proteins were eluted with maltose 10 mM diluted in buffer C. The same procedure was followed for MBP-tagged AtTPL202 wt and mutant proteins using in this case buffer D (Tris-HCl 20 mM pH 7.4, NaCl 100 mM, EDTA 1 mM, DTT 1 mM) with EDTA-free antiprotease (Roche).

GST-tagged IAA12 bacteria pellets were resuspended in buffer E (Tris-HCl 10 mM pH 8, DTT 10 mM, EDTA 1 mM, Triton 0.1%) with EDTA-free antiprotease (Roche). Soluble fractions were incubated 15 h under slow rotation speed with glutathione–resin previously equilibrated with buffer E at 4°C. Proteins were eluted with glutathione 40 mM pH 7.4 in buffer E.

Proteins dialyses were performed 15 h at 4 °C in their purification buffers and proteins were aliquoted, frozen in liquid nitrogen and stored until use at -80 °C.

Crystallization

Initial crystallization conditions were identified using the high-throughput crystallization platform at EMBL Grenoble (embl.fr/htxlab). The optimum condition for crystals of native and Se-Met TPL184 was obtained at 20 °C with the hanging drop vapour diffusion method by mixing 1 µL of protein (AtTPL184 70 µM in CAPS 133.3 mM pH 10.5, NaCl 333.3 mM, 0.66 mM TCEP and hexanediol 10% v/v) with 1 µL of reservoir

solution (Na2HPO4-Citrate 0.2 M pH 4.2, 2-propanol 10% v/v and Lithium sulfate 0.3 M). The optimum condition for crystallization of the complex AtTPL184/ IAA27 EAR motif was obtained at 20 °C with the same method by mixing 1 µL of protein (AtTPL184 140 µM, IAA27 EAR motif 1.4 mM, CAPS 20 mM pH 10.5, NaCl 50 mM and TCEP 0.1 mM) with 1 µL of reservoir solution (Di-Ammonium tartrate 1.08 M pH 7 and 2% benzamidine-HCl). Crystals were cryoprotected by plunging them into liquid nitrogen, after incubation in crystallization solution supplemented with 20% glycerol.

Protein structure determination

Se-Met protein crystallized in space group P43212 with unit cell dimensions of a=b=99.2 Å and c=290.2 Å. A SAD experiment was performed on the ESRF beamline ID29 (9) (Table 1) at the peak of the Se absorption (12.751 kEV). All data were reduced in XDS (10) within the Grenades (11) processing pipeline. The heavy atom substructure was determined and iteratively improved in SHELXC/D/E. This substructure was then refined in AUTOSHARP (12) to anomalous phasing power of 3.019 in the inner shell (58.5-12.78A) and which were greater than 1 to 4.93 Å . R_{cullis} in the inner resolution shell was 0.431 and remained below 1 to 3.08 Å. These phases were used to automatically build a model with four protomers in the asymmetric unit: 770 residues of the 848 expected. This model was partially refined and then used as a search model for molecular replacement into a higher resolution native dataset ($P3_112$, a=b=72.681 Å, c=181.147 Å, 2 protomers in the asymmetric unit, 2.6 Å resolution). Rotational and translational Z-scores of 7.1, 7.6, 12.9 and 47.2. The model was then improved through multiple rounds of manual rebuilding and refinement in COOT (13) and BUSTER (14). Data for the peptide bound structure were collected on the ESRF beamline ID23-EH2 (15). The final apo model was then used for molecular replacement to determine the structure of the IAA-peptide bound structure to 1.95 Å resolution (P43212, a=b=94.1 Å, c=298.0 Å, four protomers in the asymmetric unit). This model was completed in the same manner as the apo structure. Peptides were visible in all four binding grooves, however the electron density was significantly better in subunits A and B compared to C and D. Re-analysis of the 5C7F data was performed as follows: We applied random coordinate shifts to the 5C7F model with Phenix.dynamics to reduce bias (16), then rebuilt the peptide chain in a shifted register with COOT (13) and then refined the structure in BUSTER (14). PHENIX phenix.composite_omit_map (17) was run for both sets of data (our own and

the data downloaded for 5c7f), omitting the peptide chains and using default parameters. Figures were made in Pymol.

Native molecular mass determination

Molecular masses were determined by Size-Exclusion Chromatography-Multi Angle Light Scattering (SEC-MALLS) on an analytical Superdex-S200 increase (GE Healthcare) connected to an in-line MALLS spectrometer (DAWN HELEOS II, Wyatt Instruments). Analytical size exclusion chromatography was performed at 25ºC at a rate of 0.5 mL/min in buffer A for AtTPL184 and AtTPL202 (wt and mutants) and in buffer F (CAPS 20 mM pH 10.5, Tris-HCl 100 mM pH 8.8, NaCl 50 mM, TCEP 0.1 mM) for AtTPL202-EAR motifs complexes (fluorescence anisotropy conditions). The refractive index was measured with in-line refractive index detector (Optirex, Wyatt Instruments) was used to follow the differential refractive index relative to the solvent. Molecular masses calculation was done with the Debye model using ASTRA version 5.3.4.20 (Wyatt Instruments) and a theoretical dn/dc value of 0.185 mL/g.

Yeast two hybrid interaction tests

The vectors pGBKT7 and pACT2 were respectively transformed into yeast strains Y187 and AH109 (Clontech) using standard protocol (18). The analyses were performed after mating of the two yeast strains. Interactions were assessed using β-Gal activity (19). To do so, OD_{405nm} were measured during exponential growth phase after incubation at 30°C in Buffer G (100 mM Phosphate buffer pH 7, 10 mM KCl, 1 mM Mg_2SO_4, β-mercaptoethanol 50 mM) with ONPG.

Homogeneous-Time Resolved Fluorescence (HTRF) interaction tests

His-tagged AtTPL202 wt/mutants and MBP-tagged IAA12 interactions were analysed by HTRF (20) using CisBio Bioassays Anti-His acceptor d2 and Anti-MBP donor Tb antibodies.

HTRF experiments were performed on Greiner 384 Flat bottom wells plate. Three simultaneous replicas were done for each binding mixture. After a 2h-incubation at room temperature in the dark, the binding reactions were excited at 337 nm and emission measurements were taken at 620 nm and 665 nm with a Tecan infinite M1000PRO. HTRF specific signal was calculated as follows:

$$HTRF = \frac{Sample_{665nm}}{Sample_{620nm}} - \frac{Blank_{665nm}}{Blank_{620nm}}$$

For HTRF competition assays, an initial GST-IAA12 (200 nM) – MBP-AtTPL202 (500 nM) complex was formed using CisBio Bioassays Anti-GST donor Tb and Anti-MBP acceptor d2 antibodies. The complex formed was competed by adding increasing amounts of His-tagged AtTPL202 wt and mutant proteins. Three independent replicas were done for each binding mixture and the measurements were done in the same conditions as before.

IC_{50} were calculated fitting the competition curves to the following equation:

$$HTRF = \frac{HTRF_{max}}{1 + \frac{[AtTPL]}{IC_{50}}} + HTRF_{min}$$

Fluorescence anisotropy interaction tests

Fluorescence anisotropy interaction assays were done with wt and mutant IAA12 EAR peptides (GeneCust, Table S4) tagged to a fluorescein amidite fluorophore (FAM) at 100 nM. Increasing concentrations of AtTPL202 and mutants were added in buffer F. Three replicas per binding mixture were performed in Corning 384 Flat Bottom Black Polystyrene plates. Samples were incubated in the dark for 2 hours at room temperature. Anisotropy measurements were done with an excitation wavelength of 470 nm and an emission wavelength of 519 nm with a Tecan infinite M1000PRO.

EC_{50} were calculated fitting the binding curves using the following equation:

$$Anisotropy = \frac{Anisotropy_{Sat}[AtTPL]}{EC_{50} + [AtTPL]} + Anisotropy_0$$

Repression assays

To test the repression capacity of AtTPL202 and its mutated versions *in planta*, we used leaf mesophyll protoplasts from *Arabidopsis thaliana* (Col-0) containing the integrated reporter DR5::VENUS. Plants were grown 3 to 5 weeks in short-day condition and protoplasts were isolated and transfected using sandwich tape method and PEG method respectively (21). Protoplasts were incubated overnight in continuous light in presence or absence of 1 µM NAA. Pictures were taken with a confocal microscope Zeiss LSM710 and the fluorescence was measured using Fiji (Image J

software). Statistical analysis was tested using non-parametric Kruskal-Wallis test performed with R (http:// www.r-project.org).

Root growth and lateral root density analyses

Seeds were surface sterilized for 5 minutes in 50 % bleach, 0.1 % triton X-100 then washed three times with sterile ddH2O. Seeds were stratified at 4° for 2 days to synchronise germination. 1-week old seedlings of the indicated genotypes were transferred from normal ½ MS plates to medium complemented or not with auxin (NAA 1µM) for 5 additional days. Root growth after transfer and lateral root density were determined using Fiji (Fiji Is Just ImageJ v1.51e).

RT qPCR

1-week old seedlings of the indicated genotypes were transferred from normal ½ MS plates to medium complemented or not with auxin (NAA 1µM) for 2 hours. RNA was extracted from the whole root using the Spectrum Plant Total RNA kit (Sigma). Poly(dT) cDNA was prepared from 500 ng of total RNA with Superscript III reverse transcriptase (Invitrogen) and analyzed on a StepOnePlus apparatus (Life Technologies) with the SYBR® Green PCR Master Mix (Applied Biosystem) according to the manufacturer's instructions. Targets genes were quantified with specific primer pairs designed with the Universal Probe Library Assay Design Center (Roche Applied Science) (Table S6). All reactions were done in quadruplicate and expression levels were normalized to At1G04850 (CTRL1).

Confocal microscopy

Overexpression lines of TPL-mCherry fusions were imaged on an upright Leica SP5 confocal laser scanning microscope (Leica Microsystems, Germany). Scanner and detectors settings used at the beginning of one experiment were optimized to avoid saturation and to maximize resolution and kept unchanged throughout the experiment. mCherry was excited using a 561 nm laser and fluorescence was collected from 590 to 680 nm (using the AOBS of the SP5).

SI References

1. Kelley LA, Mezulis S, Yates CM, Wass MN, Sternberg MJE (2015) The Phyre2 web portal for protein modeling, prediction and analysis. *Nature Protoc* 10(6):845–858.

2. Corpet F (1988) Multiple sequence alignment with hierarchical clustering. *Nucleic Acids Res* 16(22):10881–10890.

3. Robert X, Gouet P (2014) Deciphering key features in protein structures with the new ENDscript server. *Nucleic Acids Res* 42(Web Server issue):W320–4.

4. Ulrich AKC, Schulz JF, Kamprad A, Schütze T, Wahl MC (2016) Structural Basis for the Functional Coupling of the Alternative Splicing Factors Smu1 and RED. *Structure*:1–12.

5. Ke J, et al. (2015) Structural basis for recognition of diverse transcriptional repressors by the TOPLESS family of corepressors. *Sci Adv* 1(6):e1500107.

6. Oberoi J, et al. (2011) Structural basis for the assembly of the SMRT/NCoR core transcriptional repression machinery. *Nat Struct Mol Biol* 18(2):177–184.

7. Chodaparambil JV, et al. (2014) Molecular functions of the TLE tetramerization domain in Wnt target gene repression. *EMBO J* 33(7):719–731.

8. Matsumura H, et al. (2012) Crystal structure of the N-terminal domain of the yeast general corepressor Tup1p and its functional implications. *J Biol Chem* 287(32):26528–26538.

9. de Sanctis D, et al. (2012) ID29: a high-intensity highly automated ESRF beamline for macromolecular crystallography experiments exploiting anomalous scattering. *J Synchr Rad* 19(Pt 3):455–461.

10. Kabsch W (2010) XDS. *Acta Crystallogr D* 66(2):125–132.

11. Monaco S, et al. (2013) Automatic processing of macromolecular crystallography X-ray diffraction data at the ESRF. *J Appl Crystallogr* 46(Pt 3):804–810.

12. Vonrhein C, Blanc E, Roversi P, Bricogne G (2007) Automated structure solution with autoSHARP. *Methods Mol Biol* 364:215–230.

13. Emsley P, Cowtan K (2004) Coot: model-building tools for molecular graphics. *Acta Crystallogr D* 60(Pt 12 Pt 1):2126–2132.

14. Bricogne G, et al. (2011) *BUSTER* (Cambridge, United Kingdom: Global Phasing Ltd.).

15. Flot D, et al. (2010) The ID23-2 structural biology microfocus beamline at the ESRF. *J Synchr Rad* 17(1):107–118.

16. Adams PD, et al. (2010) PHENIX: a comprehensive Python-based system for macromolecular structure solution. *Acta Crystallogr D* 66(2):213–221.

17. Afonine PV, et al. (2012) Towards automated crystallographic structure refinement with phenix.refine. *Acta Crystallogr D* 68(Pt 4):352–367.

18. Daniel Gietz R, Woods RA (2002) Transformation of yeast by lithium

acetate/single-stranded carrier DNA/polyethylene glycol method. *Guide to Yeast Genetics and Molecular and Cell Biology - Part B*, Methods in Enzymology. (Elsevier), pp 87–96.

19. Smale ST (2010) Beta-galactosidase assay. *Cold Spring Harbor Protocols* 2010(5):pdb.prot5423–pdb.prot5423.

20. Degorce F (2006) HTRF(®): pioneering technology for high-throughput screening. *Expert Opin Drug Discov* 1(7):753–764.

21. Wu F-H, et al. (2009) Tape-Arabidopsis Sandwich - a simpler Arabidopsis protoplast isolation method. *Plant Methods* 5(1):16.